Plant Communications
Research article

CellPress
Partner Journal

Ribosome profiling reveals the translational landscape and allele-specific translational efficiency in rice

Xi-Tong Zhu[1,3], Run Zhou[1,3], Jian Che[1], Yu-Yu Zheng[1], Muhammad Tahir ul Qamar[2], Jia-Wu Feng[1], Jianwei Zhang[1], Junxiang Gao[1,*] and Ling-Ling Chen[1,2,*]

[1]National Key Laboratory of Crop Genetic Improvement, College of Informatics, Huazhong Agricultural University, Wuhan 430070, China

[2]State Key Laboratory for Conservation and Utilization of Subtropical Agro-bioresources, College of Life Science and Technology, Guangxi University, Nanning 530004, China

[3]These authors contributed equally to this article.

***Correspondence: Junxiang Gao (gao200@mail.hzau.edu.cn), Ling-Ling Chen (llchen@gxu.edu.cn)**

https://doi.org/10.1016/j.xplc.2022.100457

ABSTRACT

Translational regulation is a critical step in the process of gene expression and governs the synthesis of proteins from mRNAs. Many studies have revealed translational regulation in plants in response to various environmental stimuli. However, there have been no studies documenting the comprehensive landscape of translational regulation and allele-specific translational efficiency in multiple plant tissues, especially those of rice, a main staple crop that feeds nearly half of the world's population. Here we used RNA sequencing and ribosome profiling data to analyze the transcriptome and translatome of an elite hybrid rice, Shanyou 63 (SY63), and its parental varieties Zhenshan 97 and Minghui 63. The results revealed that gene expression patterns varied more among tissues than among varieties at the transcriptional and translational levels. We identified 3392 upstream open reading frames (uORFs), and the uORF-containing genes were enriched in transcription factors. Only 668 of 13 492 long non-coding RNAs could be translated into peptides. Finally, we discovered numerous genes with allele-specific translational efficiency in SY63 and demonstrated that some *cis*-regulatory elements may contribute to allelic divergence in translational efficiency. Overall, these findings may improve our understanding of translational regulation in rice and provide information for molecular breeding research.

Key words: Ribo-seq, translational landscape, uORFs, lncRNAs, allele-specific translational efficiency, rice, *Oryza sativa*

Zhu X.-T., Zhou R., Che J., Zheng Y.-Y., Tahir ul Qamar M., Feng J.-W., Zhang J., Gao J., and Chen L.-L. (2023). Ribosome profiling reveals the translational landscape and allele-specific translational efficiency in rice. Plant Comm. **4**, 100457.

INTRODUCTION

Understanding the molecular basis of phenotypic variation, especially variation in gene expression, is essential for eukaryotic biology research. Transcription and translation are two critical steps in the process of gene expression (Crick, 1970). Over the past few decades, transcriptomic studies have described gene expression profiles in a wide variety of species of animals (Cardoso-Moreira et al., 2019) and plants (Klepikova and Penin, 2019), revealing the complexity of gene-regulatory networks and the evolution of gene expression patterns in different species. However, proteomics studies are lagging behind, largely because of limitations caused by the relatively low throughput of mass spectrometry (Noor et al., 2021). Ribosome profiling (Ribo-seq), a technique for deep sequencing of ribosome-protected fragments (RPFs) (Ingolia et al., 2012), enables global monitoring of translational processes *in vivo* and quantification of translated open reading frames (ORFs) in RNA; it may thus be used as a proxy for protein synthesis (Brar and Weissman, 2015). When combined with corresponding RNA sequencing (RNA-seq), Ribo-seq can be used to investigate the dynamics of translational efficiency on a genome-wide scale (Ingolia et al., 2009). Assessment of translational efficiency can

Published by the Plant Communications Shanghai Editorial Office in association with Cell Press, an imprint of Elsevier Inc., on behalf of CSPB and CEMPS, CAS.

indirectly decipher the effect of extensive translational regulation that results in poor correlations between RNA abundance and protein level (Wang et al., 2020).

Unlike mammals, plants generally exhibit broad variation within their genomes and correspondingly complex translational profiles because of several ancient whole-genome duplication events and subsequent chromosomal rearrangements (Clark and Donoghue, 2018). Understanding the role of translational changes in gene expression is more challenging but important, and many researchers have attempted to describe it in plants, particularly in *Arabidopsis* (Juntawong et al., 2014) and maize (Lei et al., 2015). More recently, a study in rice revealed the effect of nitrogen application after abrupt drought-flood alternation on translation and revealed that a fraction of genes were up- or downregulated in the translatome (Xiong et al., 2020). Researchers have also investigated the divergence in translational efficiency of alleles in hybrid yeast (Artieri and Fraser, 2014; Muzzey et al., 2014) and mice (Hou et al., 2015). For example, Hou et al. (2015) first detected over 1000 genes with allele-specific translational efficiency (ASTE) in hybrid mice and demonstrated the effects of *cis*-regulatory elements (Hou et al., 2015). However, a comprehensive study of ASTE at the single-gene level in plants remains to be performed and could help to enhance our understanding of heterosis (Zhu et al., 2021).

In this study, we performed RNA-seq and Ribo-seq experiments on leaves, panicles, and roots of three Asian rice varieties (*Oryza sativa* ssp. *xian/indica*): Minghui 63 (MH63), Zhenshan 97 (ZS97), and their elite hybrid Shanyou 63 (SY63). We compared gene expression at the transcriptional and translational levels and investigated the differences in translational efficiency (TE) among different tissues. Thousands of actively translated upstream ORFs (uORFs) and hundreds of active ORFs were detected from mRNAs and long non-coding RNAs (lncRNAs), respectively, enabling the full characterization of translational regulation in rice. Based on identified genes with ASTE, we found many genes with special translational patterns in the hybrid compared with its parents, some of which were related to agronomic traits, and some *cis*-regulatory elements on mRNAs that influenced the TE of alleles.

RESULTS

Data quality and characteristics of ribosome profiling in rice

We carried out Ribo-seq on three different tissues in three rice varieties, with two biological replicates per tissue and variety (Figure 1A). RNA-seq and Ribo-seq were carried out on the same materials, and the RNA-seq data have been published in our previous work (Zhou et al., 2021). Here, the Ribo-seq and RNA-seq data were mapped to the gap-free MH63RS3 genome (Song et al., 2021) to determine the data quality and the overall landscape of translational regulation. The mean Pearson correlation coefficient between two biological replicates was 0.92, indicating good reproducibility of our Ribo-seq data (Supplemental Figure 1A).

Ribo-seq data possess several unique features that can be used to monitor the dynamic translation process and determine the quality of the ribosome profiling libraries (Ingolia et al., 2009; Liu et al., 2013; Juntawong et al., 2014; Lei et al., 2015; Wu et al., 2019). The dominant length of RPFs reported in animals and maize (Lei et al., 2015) is 28–30 nt. However, in rice, we observed that the vast majority of RPFs were 26–28 nt in length, particularly 27 nt (Figure 1B), as also reported in a previous study (Yang et al., 2020). In total, 96.0% of the RPFs could be mapped to annotated coding sequences (CDSs), and the remaining RPFs were almost equally distributed among 5′ UTR, 3′ UTR, and intron regions (Figure 1B). In the ribosome, peptidyl elongation occurs at the P site (Lauria et al., 2018), and the estimated P-site offset varied depending on the read length (Supplemental Figure 1C). Reading frame analysis of the mapped RPFs revealed that more than 70% of them were accumulated in the first frame of the CDS (Figure 1D), whereas no enrichment of RPFs was found in the 5′ UTR or 3′ UTR. Corresponding to codon triplets, a clear 3-nt periodicity could be detected when using the first nucleotide of the P site as the position of the ribosome footprint on mRNAs (Figure 1E). There was a higher density of reads near the end regions of mRNAs, which could be attributed to the use of rare codons (Supplemental Figure 1D; Wang and Roossinck, 2006). Finally, of the 39 046 non-transposable element genes in MH63RS3, 50%–60% could be transcribed and translated (Figure 1F), consistent with a previous report (Zhao et al., 2017). When transcribed, an average of 85% of the genes would recruit the ribosome complex for translation (Supplemental Table 1), indicating the protein-coding function of these genes. These results suggested that our Ribo-seq libraries for all three varieties and tissues were of high quality (Dunn et al., 2013; Fields et al., 2015) and suitable for further analysis.

Expression changes at transcriptional and translational levels

Based on the transcriptome and translatome data, we first investigated the global differences in gene expression patterns among different varieties and tissues. There were high correlations (∼0.95; Supplemental Figure 2A and Supplemental Methods 2) between the normalized expression values (TPM, transcripts per million) generated from 150-bp paired-end reads and simulated 30-bp single-end reads, indicating that the length of RNA-seq reads would cause little bias in the analysis results and that the computation of TE was appropriate, regardless of the difference in sequenced read length (Lei et al., 2015). Next we computed the expression variance at both levels to measure the effects of transcriptional or translational regulation on gene expression (Wang et al., 2020). Various types of post-transcriptional modifications can regulate gene expression by modulating TE, leading to higher expression variance in the translatome (Csárdi et al., 2015; Weinberg et al., 2016). We found that the expression variances in the translatome were higher than those in the transcriptome for all varieties and tissues (Figure 2A and 2B and Supplemental Figure 2B). On average, the Ribo-seq variances for the leaf, panicle, and root were ∼0.733, ∼0.858, and ∼0.793, about 8.39%–25.3% higher than those of RNA-seq (Figure 2B). Genome-wide analysis of the TE variation range showed that the panicle had the broadest TE range (∼167-fold), but no consistent pattern was observed for the three varieties (Supplemental Figure 2C). By contrast, the overall TE distribution displayed a clear tissue-specific

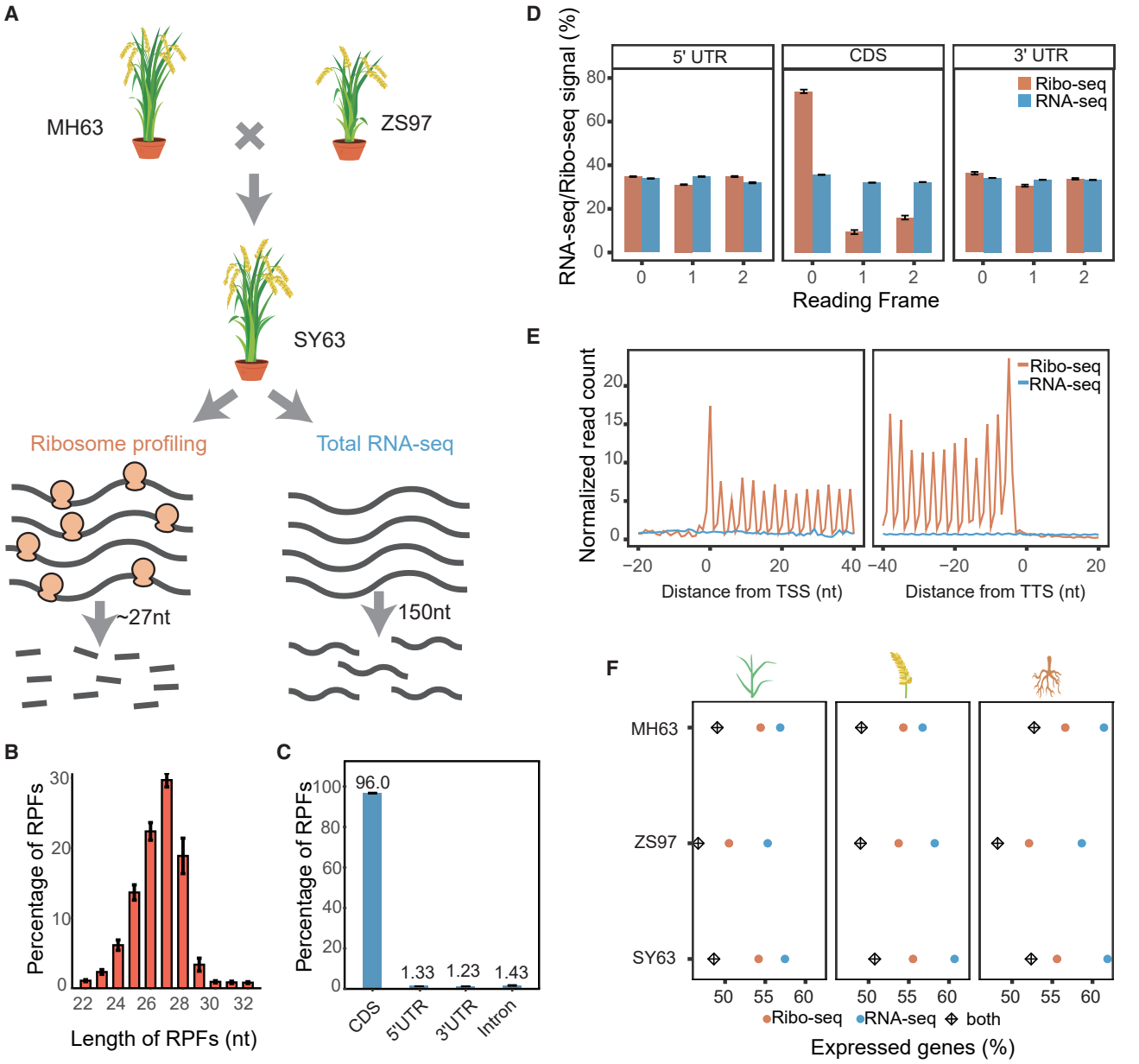

Figure 1. Deep sequencing-based global quantification of parents and hybrids.

(A) Brief overview of the experimental design. Detailed protocols for the Ribo-seq and RNA-seq experiments can be found under methods.

(B) Length distribution of Ribo-seq ribosome-protected fragments (RPFs) with a peak at 27 nt.

(C) The proportion of RPFs within annotated genes, ~96% of which are located in the CDS region.

(D) Reading frames of optimally mapped Ribo-seq reads and RNA-seq reads within annotated genes.

(E) Distribution of optimally mapped reads along the CDS within each codon. Each read was represented by a specific P-site position depending on its fragment length. TSS, translation start site; TTS, translation termination site.

(F) The proportion of expressed genes (TPM > 0.1) at the translatome level (orange), transcriptome level (blue), and both levels across tissues and varieties.

Data in **(B)–(E)** were calculated for each replicate and aggregated. RPFs with a size of 25–31 nt were used in **(D)** and **(E)**. Error bars display ±SEM.

pattern: the leaf had higher TE than the other two tissues (Figure 2C), which probably reflected an optimized usage of TE favored by each tissue, as observed in animals (Waldman et al., 2010). Next we conducted a Gene Ontology (GO) enrichment analysis and found functional divergence between genes with high and low translation (Figure 2D and Supplemental Data 2), indicating that some specific genes are strongly influenced by translational regulation (Lei et al., 2015; Wang et al., 2020) in rice. Although there were relatively high correlations of gene expression between the two levels (Supplemental Figure 3), TE and RNA abundance were relatively weakly associated (Supplemental Figure 2D and 2E). These results suggest that TE can be used as an indicator to study gene expression regulation in rice.

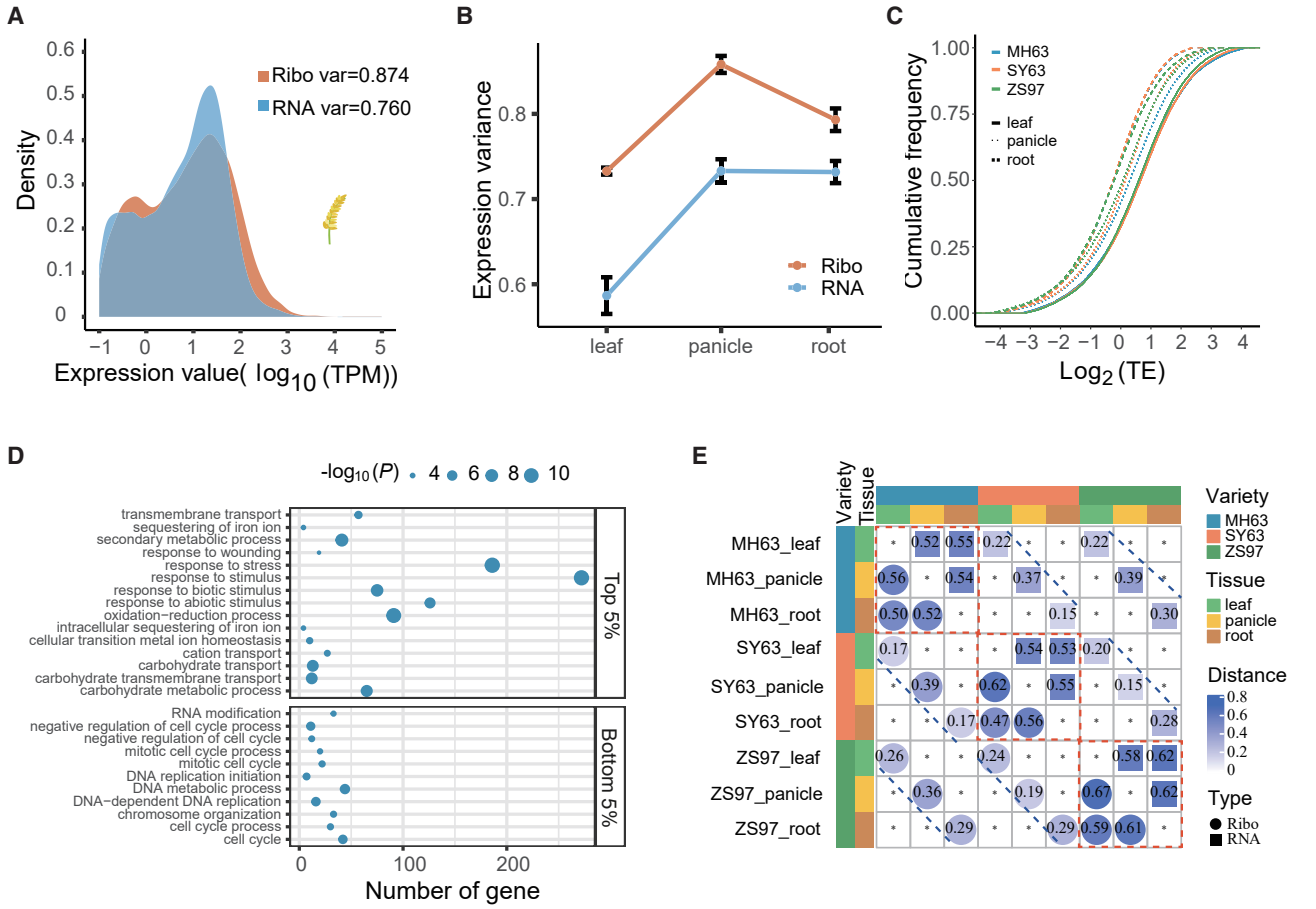

Figure 2. Gene expression divergence between the transcriptome and translatome.

(A) The distribution of expression values at the translational level in panicles of SY63 compared with that at the transcriptional level. The expression variance at the translational level is greater than that of the transcriptome.

(B) The expression variances were calculated for the translatome and transcriptome levels across tissues and varieties. Error bars indicate ±SEM.

(C) Cumulative distribution of TE for protein-coding genes expressed across tissues and varieties.

(D) GO enrichment results for the top 5% and bottom 5% TE genes in MH63 leaves. Only biological process terms are shown.

(E) Euclidean distances of expression profiles at the translational and transcriptional levels across tissues and varieties.

We calculated the divergence of expression profiles between or within the transcriptional and translational levels for all varieties and tissues. In Figure 2E, the squares and circles represent the gene expression distances at the two levels. The data in the three red dashed boxes and along the blue dashed lines represent the expression distances of RNA-seq and Ribo-seq in different tissues of the same variety and the same tissue of different varieties, respectively. The expression distances in the red dashed boxes are significantly larger than those on the blue dashed lines at the transcriptional and translational levels. In general, the inter-tissue expression distances within a variety were much larger than the inter-variety distances within a tissue, suggesting that a given tissue has similar transcriptional and translational regulatory mechanisms among different varieties. The transcription distance or translation distance in the same tissue was roughly equal between varieties. To quantify the contribution of transcriptional or translational regulation to gene expression and explore the potential effects of this regulation on shaping phenotypic diversity, we performed differential expression analyses between different tissues of the same variety (inter-tissue) and between the same tissue in different varieties (intra-tissue).

In general, we found that the number of differentially expressed genes in the transcriptome (RNA_only) was approximately 2.39 times higher than that in the translatome (Ribo_only; 3616 versus 1516; Supplemental Figure 4), suggesting that more genes were subjected to regulation at the transcriptional level. However, GO enrichment results for Ribo_only genes revealed that they were involved in a number of crucial biological processes, some of which may be closely related to tissue-specific or variety-specific phenotypes (Supplemental Data 3). For example, "reproduction" (GO:0000003; P = 4.59e−04) was enriched in the comparison of panicle and root, suggesting that some genes dominantly regulated by translation are associated with reproductive growth, as the panicle is known as the beginning of the reproductive phase of rice development (Li et al., 2021). ZS97 usually grows much faster than MH63 at the seedling stage (Xu et al., 2004), and we found that some GO terms were enriched in the comparison of MH63 and ZS97, such as "generation of precursor metabolites and energy" (GO:0006091; P = 0.0209), which may be linked to this phenotypic difference. Although fewer genes were dominantly regulated by translation, their notably enriched functions

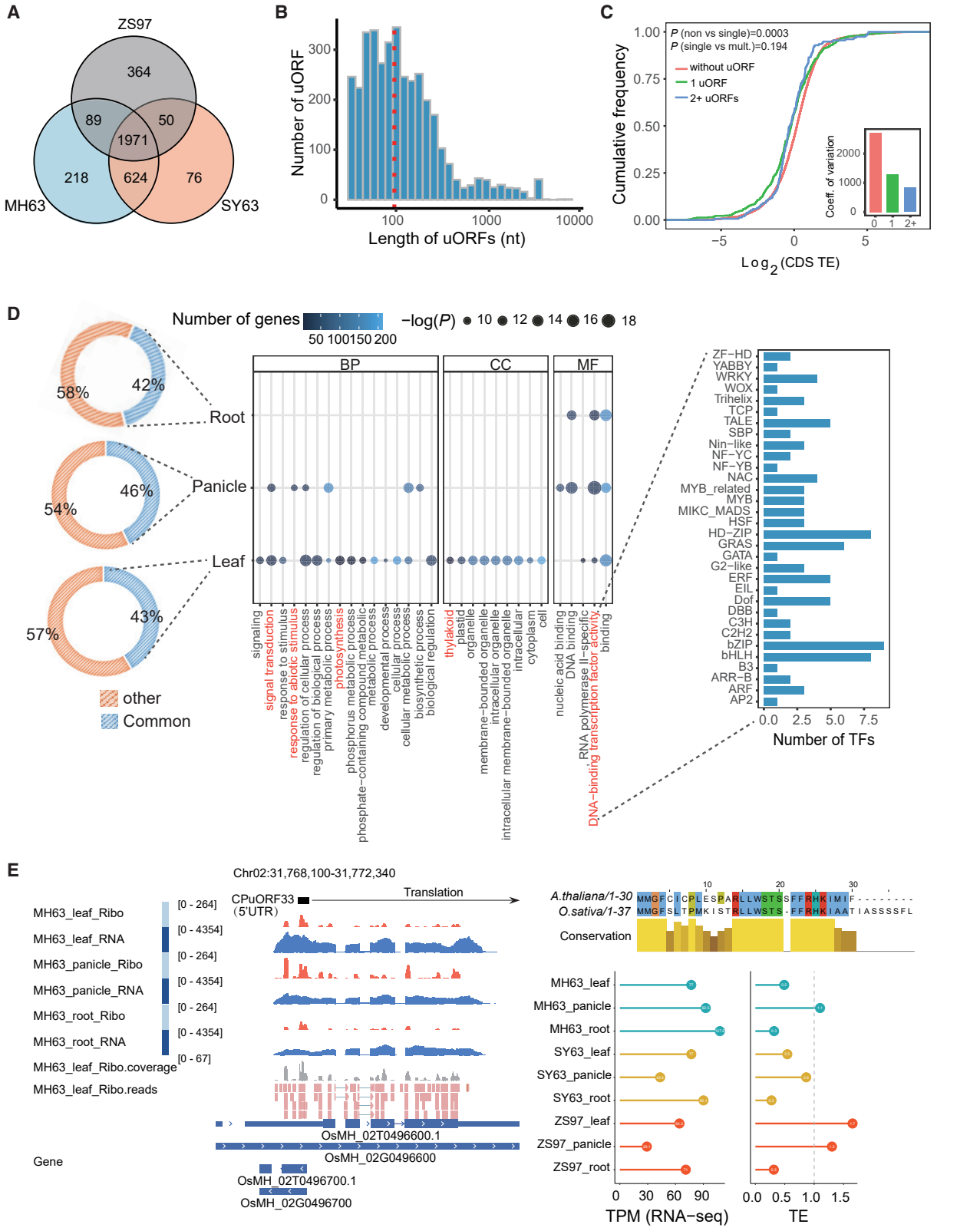

Figure 3. uORF-mediated translational regulation.

(A) Three-way Venn diagram showing the numbers of uORFs shared by the three varieties.

(B) Length distribution of the translated uORFs, with a median length of 96 nt (red dashed line).

(legend continued on next page)

suggest that translational regulation plays important roles in rice development.

Regulation of translation by uORFs in rice

Although a previous study identified thousands of uORFs in rice, that work focused mainly on the effect of abrupt drought-flood alternation (Xiong et al., 2020). Here, we comprehensively characterized uORFs among three varieties and different tissues. In total, 2902, 2474, and 2912 uORFs were identified in MH63, ZS97, and SY63, respectively (Supplemental Table 2 and Supplemental Data 4). Although each variety harbored hundreds of unique active uORFs, about two-thirds of the uORFs were shared by all three varieties (Figure 3A), indicating that these uORFs are necessary and may participate in important cellular processes. As expected, the length of active uORFs was shorter than that of main ORFs (mORFs), with a median value of 96 nt (Figure 3B and Supplemental Figure 5A). The core function of uORFs is to suppress translation of mORFs in animals (Calvo et al., 2009; Ingolia, 2014) and plants such as maize (Lei et al., 2015). However, it has been reported that genes with one uORF have a TE similar to that of genes without uORFs; when the number of uORFs increases to two or more, the uORFs can improve the TE of their mORFs in young rice leaves (Xiong et al., 2020). Here, we calculated the cumulative distribution of TE and found a tissue-specific pattern in the regulatory effect of uORFs on mORFs. In the root, the TE of mORFs with one or more uORFs decreased (Figure 3C and Supplemental Figure 5B). However, in the leaf and panicle, the cumulative distribution curves for mORFs without or with one or more uORFs largely overlapped, indicating that the presence and number of uORFs did not significantly alter the TE of mORFs (Supplemental Figure 5B). These distinct regulatory patterns among tissues were also confirmed using more reliable uORFs identified with RiboTaper (Supplemental Figure 6), although the number of uORFs was much smaller (Supplemental Data 3), probably because of the strict inbuilt 3-nt periodicity criterion, which required a higher sequence depth (Calviello et al., 2016). We also calculated the coefficient of variation of TE to evaluate the effects of uORFs. The coefficients of variation of TE were higher for genes without uORFs than for genes with one or more uORFs across all varieties and tissues (Figure 3C and Supplemental Figure 5C). This was consistent with another function of uORFs found in *Drosophila melanogaster* (Patraquim et al., 2020), in which uORFs were reported to buffer the translation of mORFs, leading to lower dispersion of TEs.

Considering that a large proportion of uORFs were shared by all samples (Figure 3D), we performed a GO enrichment analysis to understand the potential functions of these uORF-containing genes. As shown in Figure 3D, although some GO terms were tissue specific, "DNA-binding transcription factor activity" (GO: 0003700, P_{max} = 1.94e−04) was significantly enriched for all three tissues, indicating that these genes play certain roles as transcription factors (TFs). By searching plant TF databases, we found that many uORF-containing genes harbor various TF DNA-binding domains, as shown in the right panel of Figure 3D. Some of these genes may be vital for plant development. For example, *OsMH_02G0496600* is the homolog of *Arabidopsis ATHB1* (*AT3G01470*), which encodes a homeodomain-leucine zipper domain TF. Overexpression of *ATHBI* in *Arabidopsis* causes deleterious phenotypes such as serrated leaves, and a uORF (CPuORF33) can repress translation of this TF via a ribosome stalling mechanism in aerial tissues of *Arabidopsis* (Ribone et al., 2017). A DNA sequence similar to this uORF was identified in rice, and the two uORFs had relatively high identity (66.7%; Figure 3E). The expression profile showed that the mORF of this gene was expressed in all tissues (Figure 3E; Supplemental Data 4), but the TE was low in most tissues (in the bottom 20% of all translated genes on average), indicating that the presence of CPuORF33 homologs may contribute to this low TE. These results suggest that the identified uORFs have multiple roles in rice, some of which may be important for gene regulation; they can also serve as a valuable resource for further experimental studies.

Translation ability of lncRNAs in rice

To understand the translation ability of the widely distributed lncRNAs reported in our previous work (Zhou et al., 2021), we re-identified the lncRNAs in the MH63RS3 genome using the same pipeline and predicted their coding potential. In total, only 4.95% (668) of all lncRNAs with one or more active ORFs could be translated (Figure 4A and Supplemental Data 5), suggesting that the identification of a majority of lncRNAs in our previous study is reliable and that translation of lncRNAs is not universal in rice. Although these active ORFs had a greater median length (237 nt) than uORFs, they were still significantly shorter than ORFs from protein-coding genes (Figure 4B and Supplemental Figure 5A). Five types of lncRNAs have been classified previously, and we found that 60.3% of active ORFs were derived from long intergenic noncoding RNAs, followed by long noncoding natural antisense transcripts (23.4%; Figure 4C). Considering the poor conservation of lncRNAs among varieties (Zhou et al., 2021) and the relatively large number of shared active translational ORFs among varieties and tissues (Supplemental Figure 7A), we speculate that these lncRNAs may have functions similar to protein-coding genes.

To validate this speculation, we performed *de novo* functional annotation of 834 active ORFs in lncRNAs using three approaches (Figure 4D and Supplemental Data 5). First, we

(C) Cumulative distribution of CDS TEs in mORFs and coefficients of variation (inset) grouped by uORF number in the root of SY63. Kolmogorov–Smirnov test *P* values are labeled.

(D) GO terms and TF categories of uORF-containing genes shared by the three varieties in different tissues. The left panel shows the proportion of uORFs shared by the three varieties across tissues. The right panel shows the GO terms of the uORF-containing genes shared by the three varieties across tissues.

(E) The gene *OsMH_02G0496600*, a homolog of *ATHB1* in *Arabidopsis*, contains the same uORF, CPuORF33, which also inhibits translation of the mORF. The Ribo-seq and RNA-seq signals from leaf, panicle, and root of MH63 are shown in the left panel (only tissues from MH63 are shown). The raw reads from the MH63 leaf are also shown to explain that these signals are from CPuORF33, not the anti-sense gene *OsMH_02G0496700*. The protein sequence comparison of CPuORF33 in *Arabidopsis* and rice is shown at the top right, and the expression level and TE of the mORF in *OsMH_02G0496600* are shown at the bottom right.

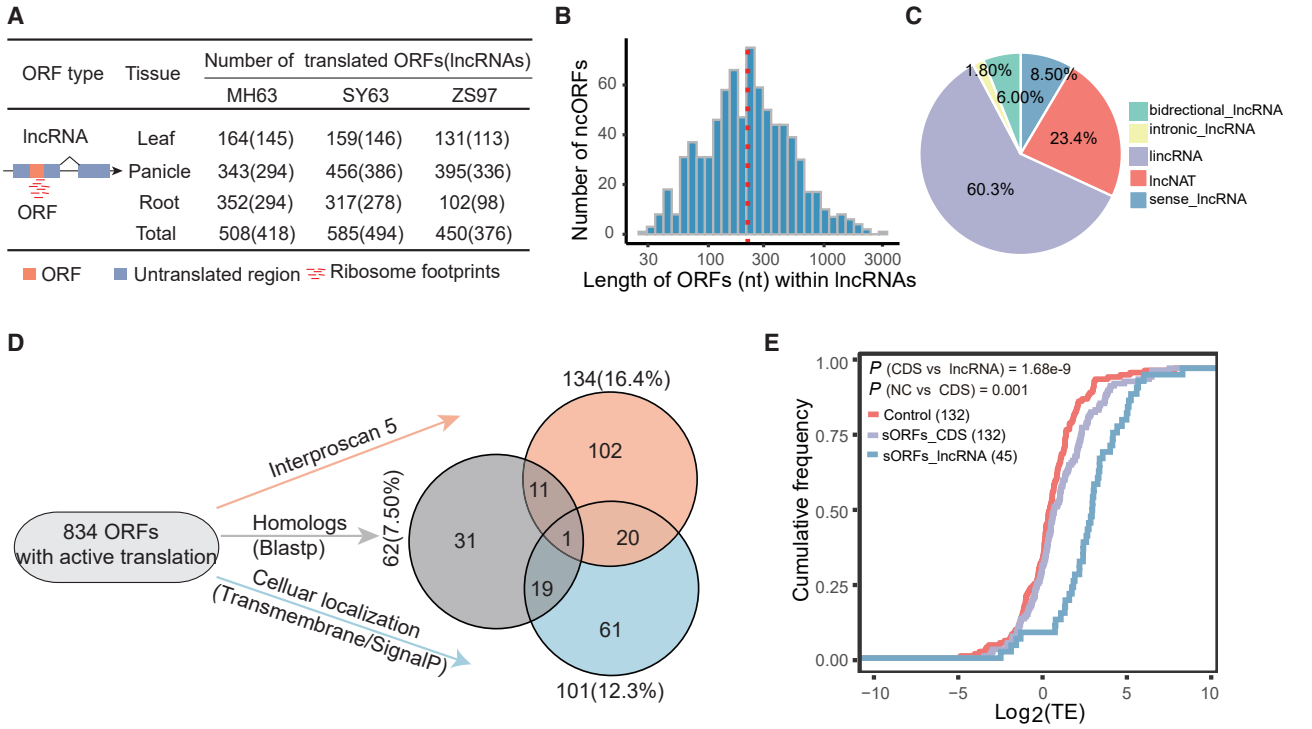

Figure 4. Translation of lncRNA genes.

(A) The number of actively translated ORFs in lncRNAs identified in each tissue and variety.

(B) Length distribution of active ORFs, with a median length of 237 nt (red dashed line).

(C) Pie chart of lncRNA categories containing active ORFs.

(D) Functional annotation of active ORFs. The Venn diagram shows the overlapping numbers of active ORFs identified using three different strategies. See methods for details.

(E) Cumulative distribution of TEs of lncRNAs with sORFs compared with protein-coding genes with sORFs in leaves of MH63. A sample of randomly selected protein-coding genes whose CDS lengths were greater than 300 nt was used as a control. Kolmogorov–Smirnov test *P* values between different kinds of genes are labeled.

searched multiple protein databases using InterProScan 5 (Jones et al., 2014) and found that 16.1% (134) of the 834 active ORFs contained one or more conserved domains. Second, we found that 62 (7.43%) active ORFs had high sequence similarity to known proteins by searching against all annotated small proteins (shorter than 100 amino acids [aa]) in the MH63RS3 genome. Third, because small proteins can function as signal peptides in a wide range of plant species (Matsubayashi, 2014), we predicted the transmembrane topology and signal peptide structure of these active ORFs and found that 101 (12.1%) might be located on the membrane (82) or secreted (31).

Considering the relatively short lengths of active ORFs (Supplemental Figure 7B), we next attempted to determine whether there were differences between active ORFs and mRNAs that contained small ORFs (sORFs; CDS shorter than 300 nt), such as differences in TE. We found that 243, 292, and 206 lncRNAs and 300, 286, and 259 mRNAs could be translated into small peptides in MH63, SY63, and ZS97, respectively (Supplemental Table 3). We then compared the TE of sORFs from mRNAs and lncRNAs. The results showed that active ORFs had higher TE than mRNAs (Figure 4E and Supplemental Figure 7C). The sORFs in lncRNAs were shorter in length and higher in TE in all tissues (Supplemental Figure 8A), and we speculated that this higher TE could be partly attributed to the shorter length of these sORFs (Zhao et al., 2017). We also observed that the translation of these sORFs in lncRNAs tended to use rare codons compared with those in mRNAs (Supplemental Figure 8B).

Identification of genes with ASTE in hybrid rice

In addition to the above findings, our data can also be used to determine the TE divergence between allelic genes in the hybrid SY63 and identify *cis*-regulatory elements that are responsible for such divergence. Because both allelic genes in a hybrid are influenced by the same *trans*-acting factors (such as TFs and microRNAs [miRNAs]), the observed TE divergence in alleles may be caused by *cis*-regulatory elements in mRNAs, such as GC content, secondary structure, and miRNA binding sites (McManus et al., 2014). To test this possibility, it is crucial to assign sequenced reads to definite parental alleles. We designed a pipeline to obtain such reads and identified genes with ASTE (Figure 5A; methods). The phasing separation rate for RNA-seq was 14.90% on average, whereas fewer reads from Ribo-seq could be phased (1.49%); this can be explained intuitively by their short length (~30 nt), which results in a small probability of containing SNPs. However, the average phasing error rates for RNA-seq and Ribo-seq were 1.13% and 2.10% (Supplemental Table 4 and Supplemental Data 5), respectively, indicating a

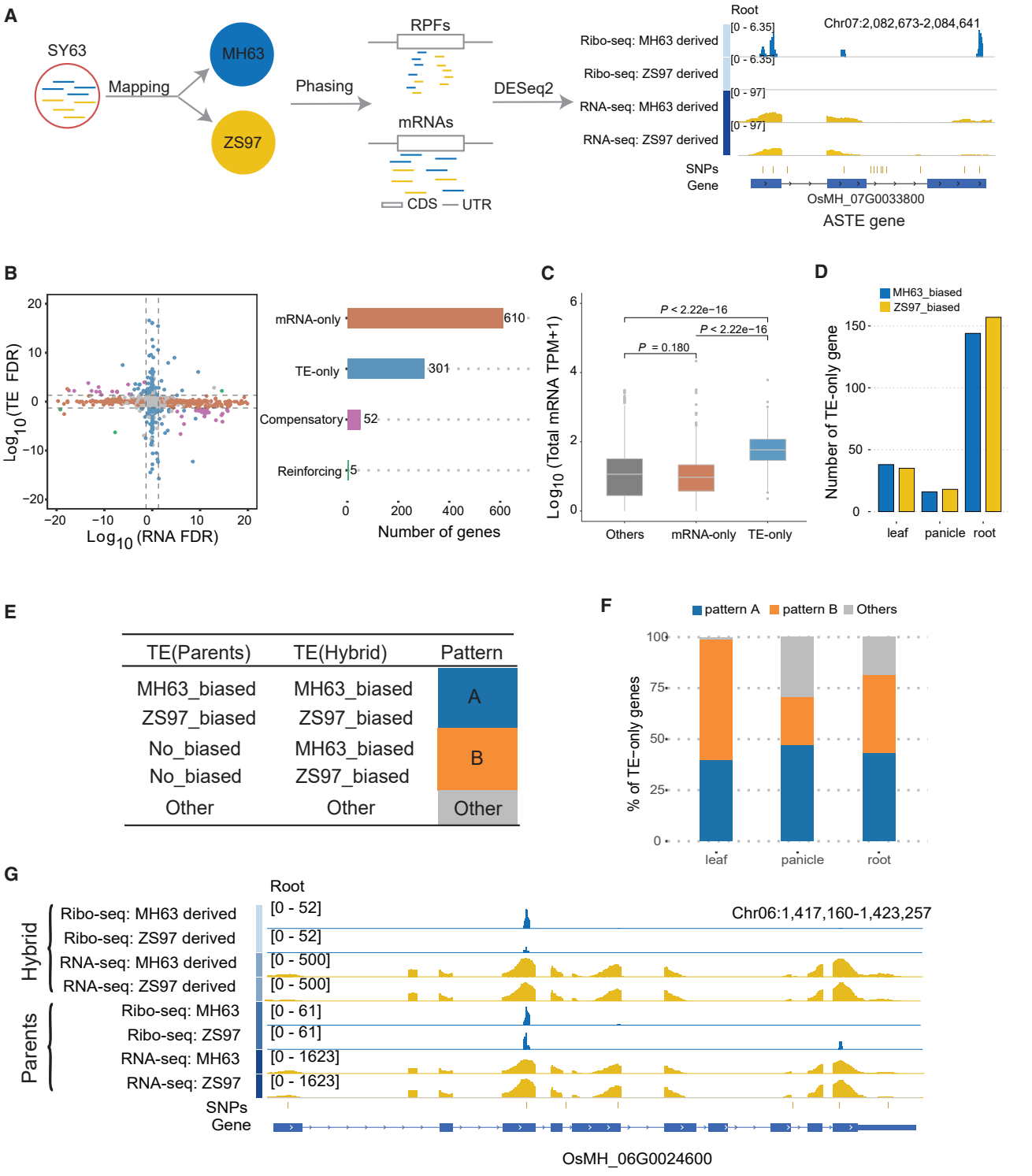

Figure 5. Characteristics of genes with ASTE.

(A) The left panel shows the pipeline used to identify genes with ASTE, including read mapping, phasing with PP2PG, and difference detection by DESeq2. See methods for details. The right panel shows an example of a gene with ASTE. Gene *OsMH_07G0033800* is shown with Ribo-seq and RNA-seq signals from both alleles. Four of five SNPs in the CDS region are covered by Ribo-seq reads in the MH63 allele, indicating a reliable divergence in allelic TE.

(B) Relationships between TE and RNA abundance in genes with allelic expression bias in root tissue. The false discovery rate (FDR) for each gene represented by each point in the left panel was adjusted according to its fold change: $-log_{10}(FDR)$ *if* $FC(ZS97/MH63)>0$; $log_{10}(FDR)$ *if* $FC(ZS97/MH63)<0$ at the mRNA or TE level. The right panel shows the numbers of different kinds of genes in the left panel.

(legend continued on next page)

comparable accuracy for Ribo-seq reads without being compromised by a low separation rate. The phased reads also showed high correlations between replicates (on average 0.953 and 0.947 for Ribo-seq and RNA-seq, respectively; Supplemental Figure 9). We then selected 14 659 genes containing SNPs within their CDS region from all 1:1 orthologs between MH63 and ZS97 to identify genes with significant ASTE. Under the cutoff false discovery rate $FDR \leq 0.05$ and $|log_2(Fold\ change)| \geq 1$, we identified 420 genes with ASTE, including 81, 36, and 358 in the leaf, panicle, and root of SY63, respectively (Supplemental Data 7 and 8). Only a few ASTE genes were shared by all three tissues (Supplemental Figure 10A). The right panel of Figure 5A shows a representative example. The *ONAC096* (*OsMH_07G0033800*/*LOC_Os07g04510*) gene, which belongs to the NAM, ATAF and CUC (NAC) TF superfamily (Puranik et al., 2012), has been reported to mediate abscisic acid-induced leaf senescence and improve grain yield (Kang et al., 2019). Expression of this gene at the RNA-seq level was high in the root but low in the panicle in all three varieties (Supplemental Figure 10B), consistent with the finding of Kang et al. (2019). However, further examination at the translational level in the hybrid showed that the Ribo-seq signal from the MH63 allele was much stronger than that from ZS97, indicating strong allelic specificity of this gene at the translational level (Supplemental Figure 10C).

Previous studies have reported multiple patterns of allelic regulation at the transcriptional and translational levels in yeast (Artieri and Fraser, 2014) and mice (Hou et al., 2015). Thus, we also explored this phenomenon in rice by taking the root as an example because it had the largest number of ASTE genes (358). Following the procedures in a previous study (Hou et al., 2015), all genes with allelic bias were classified into four categories (Supplemental Data 9). Among these genes, 610 showed significant allelic specificity only in mRNA abundance (hereafter referred to as mRNA-only genes). By contrast, 301 genes had significant allelic specificity only in TE (hereafter referred to as TE-only genes). Another 57 genes had allelic specificity in mRNA abundance and TE. As shown in Figure 5A and 5B, a positive coordinate value indicates that the gene was biased to ZS97, and a negative coordinate value suggests that the gene was biased to MH63. Among these 57 genes, 52 were in the second and fourth quadrants, exhibiting a compensatory effect of transcription and translation, and these were called compensatory genes. This regulatory pattern may be used by hybrids to maintain equal protein levels of the two alleles. Another five genes were in the first and third quadrants, showing a reinforcing effect of the transcription and translation processes, and were designated reinforcing genes.

We compared the transcription level between mRNA-only and TE-only genes in all three tissues. The results showed that TE-only genes had significantly higher total mRNA abundance (Figure 5C and Supplemental Figure 10D and 10E), suggesting that allele-specific translational regulation occurred preferentially on mRNAs with higher abundance. TE-only genes were involved in various processes, like "response to stimulus" (GO:0050896, P = 4.69e–05), whereas very few enriched functions were found for mRNA-only genes (Supplemental Figure 12A and Supplemental Data 10). Last, we categorized the TE-only genes into MH63-biased or ZS97-biased types and found that, in all three tissues of SY63, these two types of genes were highly similar in number (Figure 5D).

To understand the potential role of translational regulation in heterosis, we analyzed the TE-biased patterns of all TE-only genes among the parents and the hybrid variety (Figure 5A; methods). The TE of the two alleles of a TE-only gene in the hybrid had three possible patterns, MH63 biased, ZS97 biased, and no bias (Figure 5E), and it was similar for a TE-only gene between the two parents. In total, the TE bias of the hybrid and parents had nine possible combinations, four of which accounted for a large proportion of the TE-only genes (Supplemental Data 11) and were named pattern A and pattern B (Figure 5E). In pattern A, the hybrid and parents had the same TE bias, whereas in pattern B, the TE changed from no bias to biased toward one allele. Pattern A comprised 43.3% of the total TE-only genes on average (Figure 5F). Among these genes, 87.2% could be functionally annotated, a higher percentage than that of randomly selected genes (Fisher's exact test, P = 0.009482). Among genes with similar regulatory patterns, several genes experimentally validated as associated with disease resistance tended to show high TE in the MH63 allele, such as *OsHIR1* (Zhou et al., 2010) and *OsLOX3* (Marla and Singh, 2012; Supplemental Figure 11A and 11B). MH63 has been reported to be resistant to multiple rice diseases, such as blast disease (Xie and Zhang, 2018). Therefore, this similar regulatory pattern is very likely related to the disease resistance phenotype of hybrid SY63 inherited from MH63. Another gene, *OsMH_09G0296900*, was biased toward ZS97 at the TE level and identified as a transporter of cytokinin in rice (Supplemental Figure 11C). The protein encoded by this gene may promote the growth of rice and may therefore play an important role in the faster growth of ZS97 and SY63 compared with MH63 at the early seedling stage (Xu et al., 2004). Pattern B included approximately 40.1% of the total TE-only genes (Figure 5F). A large proportion of these genes could be functionally annotated (Supplemental Data 11). For example, the gene *OsMH_06G0024600* (*LOC_Os06g03860*) was switched to higher TE in the MH63 allele in the root of SY63; it encodes a phosphate (Pi) transporter

(C) Comparison of total mRNA expression levels among three kinds of genes in root tissue. Wilcoxon test P values are labeled. The numbers of mRNA-only and TE-only genes are displayed in **(B)**. Other genes, equal in number to the set of mRNA-only genes, were randomly selected from genes that were not in one of the four categories.

(D) The numbers of MH63-biased or ZS97-biased TE-only genes in three tissues of SY63.

(E) Two major regulatory patterns exhibited in TE-only genes. In pattern A, differences in TE levels are the same in the parents and the hybrid, whereas in pattern B, the TE level is biased toward one allele.

(F) Number of TE-only genes with different patterns in three tissues of SY63.

(G) RNA-seq and Ribo-seq signals for gene *OsSPX-MFS3* (*OsMH_06G0024600*/*LOC_Os06g03860*) in the hybrid (first four tracks) and parents (next four tracks); the gene shows higher TE of the MH63 allele in the hybrid (pattern B) and has been reported to participate in maintaining phosphate homeostasis in rice.

involved in maintaining cytosolic Phosphate concentration in rice (Qi and Xiong, 2013; Figure 5G). Although the role of allele-specific expression in heterosis has been studied mainly at the transcriptional level, our finding that these two patterns only change in TE may provide a new perspective for studying the role of allele-specific expression in heterosis at the translational level.

cis-regulatory elements related to divergence of allelic TE

To study the role of *cis*-regulatory elements in determining the divergence of TE-only genes, 361 genes were used for further analyses. We first compared the sequence variations between TE-only genes and those without allelic TE divergence (hereafter referred to as control genes; Figure 6). The TE-only genes had more SNPs than the control genes (Figure 6A). Also, a higher SNP density was observed in the TE-only genes (3.15 versus 2.40 SNP/kb; Figure 6B; Wilcoxon test, $P = 2.43e{-}05$). In both types of genes, SNPs were enriched in UTRs (Figure 6C). Compared with the control genes, TE-only genes had slightly more SNPs within their 5′ UTRs but many more SNPs in the CDS and 3′ UTR regions. In the region near the start codon, we also found more SNPs in TE-only genes (Supplemental Figure 12B).

We next took several *cis*-regulatory elements into account to study their contribution to the TE divergence of alleles. GC content around the start codon, as a basic feature, did not differ between TE-only genes and control genes (Figure 6D; mean GC content, 0.604 versus 0.587; Wilcoxon test, $P = 0.108$). The Kozak sequence (Kozak, 1987) has been reported to control the translational process in multiple ways (Hata et al., 2021). We found that 18 TE-only genes (accounting for 5%) showed variations in their Kozak sequence, as did 11 control genes (accounting for 3.05%), and this difference was not significant (Fisher's exact test, $P = 0.255$; Supplemental Table 5). In addition, no significant difference was observed in the position around the start codon (Figure 6E). Another important factor that may influence TE is the secondary structure of mRNAs (Hall et al., 1982). We predicted the minimum free energy (MFE) of each mRNA around the start codon. The results showed that the TE-only genes had a significantly lower MFE than the control genes (Figure 6F; Wilcoxon test, $P = 2.84e{-}05$), suggesting that genes with allelic TE divergence tend to possess a more stable secondary structure. It has been reported that codon usage can regulate the speed of ribosome movement on mRNAs and, thus, influence TE (Wang and Roossinck, 2006). We found that TE-only genes tended to use more optimal codons with high frequencies compared with control genes (Supplemental Figure 12C; Wilcoxon test, $P = 2.98e{-}04$). Moreover, 11.9% of TE-only genes contained at least one uORF, a percentage that did not differ significantly from that of control genes (7.11%; Fisher's exact test, $P = 0.134$). There were also no significant differences in the number of uORFs in these two types of genes (Figure 6G).

Finally, we checked the differences in miRNA binding sites because many previous studies have highlighted the importance of miRNAs in controlling translation in plants (Brodersen et al., 2008; Iwakawa and Tomari, 2013; Song et al., 2019). We detected no significant differences in the number of miRNA binding sites between TE-only and control genes (Figure 6H; Wilcoxon test, $P = 0.701$). However, we still suspected that binding site divergence within a pair of alleles could contribute to allelic TE divergence. We therefore predicted the genome-wide miRNA binding sites on MH63 and ZS97 genes. The results showed that 17.5% of TE-only genes showed differences between the two alleles (Supplemental Data 12). For example, *OsMH_12G0321800/OsZS_12G0351200*, which showed tissue-specific expression in roots (Supplemental Figure 12D), contained a binding site for osa-miR6249 only in the CDS region of the MH63 allele (Figure 6I). The Ribo-seq signal derived from the MH63 allele was significantly lower than that from the ZS97 allele, whereas almost equal RNA-seq signals were detected (Figure 6I), indicating reduced TE on the MH63-derived allele.

Further examination revealed that one SNP (chromosome 12: 22745704–22745705 in the MH63RS3 genome) may be responsible for the difference in binding sites between the two alleles (Figure 6I and 6J). The predicted mRNA secondary structures around this SNP site for the two alleles were clearly different (Supplemental Figure 12E). To validate this binding difference, a luciferase reporter assay was performed for the two homologous genes in protoplasts of hybrid SY63 (Supplemental Methods 4). Transfection of the miRNA osa-miR6249 significantly reduced the luciferase activity of the target gene only in the MH63 allele but not in the ZS97 allele (Figure 6K and Supplemental Data 13). This decreased luciferase activity could come from miRNA-mediated mRNA degradation, translational repression by prevention of ribosome elongation, or a combination of both (Iwakawa and Tomari, 2013; Kaur et al., 2020), thereby enabling the detection of altered TE. Therefore, we can speculate that the binding difference of this miRNA may be responsible for the observed TE divergence between these two alleles.

DISCUSSION

Protein synthesis level has been shown to correlate poorly with mRNA abundance in eukaryotic organisms (Ingolia et al., 2009; Battle et al., 2015), a phenomenon that may be largely ascribed to translational regulation (Urquidi Camacho et al., 2020). In this study, by analysis of three tissues in two parental varieties and their hybrid, we provide a comprehensive profile of translational regulation and allelic TE divergence in rice. We found some interesting regulatory patterns at the translational level. When measuring the overall level of TE, the root showed the lowest TE level (Figure 2C) compared with the panicle and leaf. This may be attributed to some overall unique features of expressed genes at the early stage of rice development, such as the shorter poly(A) tail length that represses translation, as observed in animals (Subtelny et al., 2014). A study using a more accurate poly(A) enrichment-free and nanopore-based method found that, in *Arabidopsis*, poly(A) tail length was much shorter in the root (Jia et al., 2022). However, comparison of the dispersion of expression across genes at the translational level led to the finding that the panicle showed increased variance (Figure 2B). This result may reflect the strong translational impacts of some newly involved genes, such as those related to reproduction, as the panicle represents the initial stage of

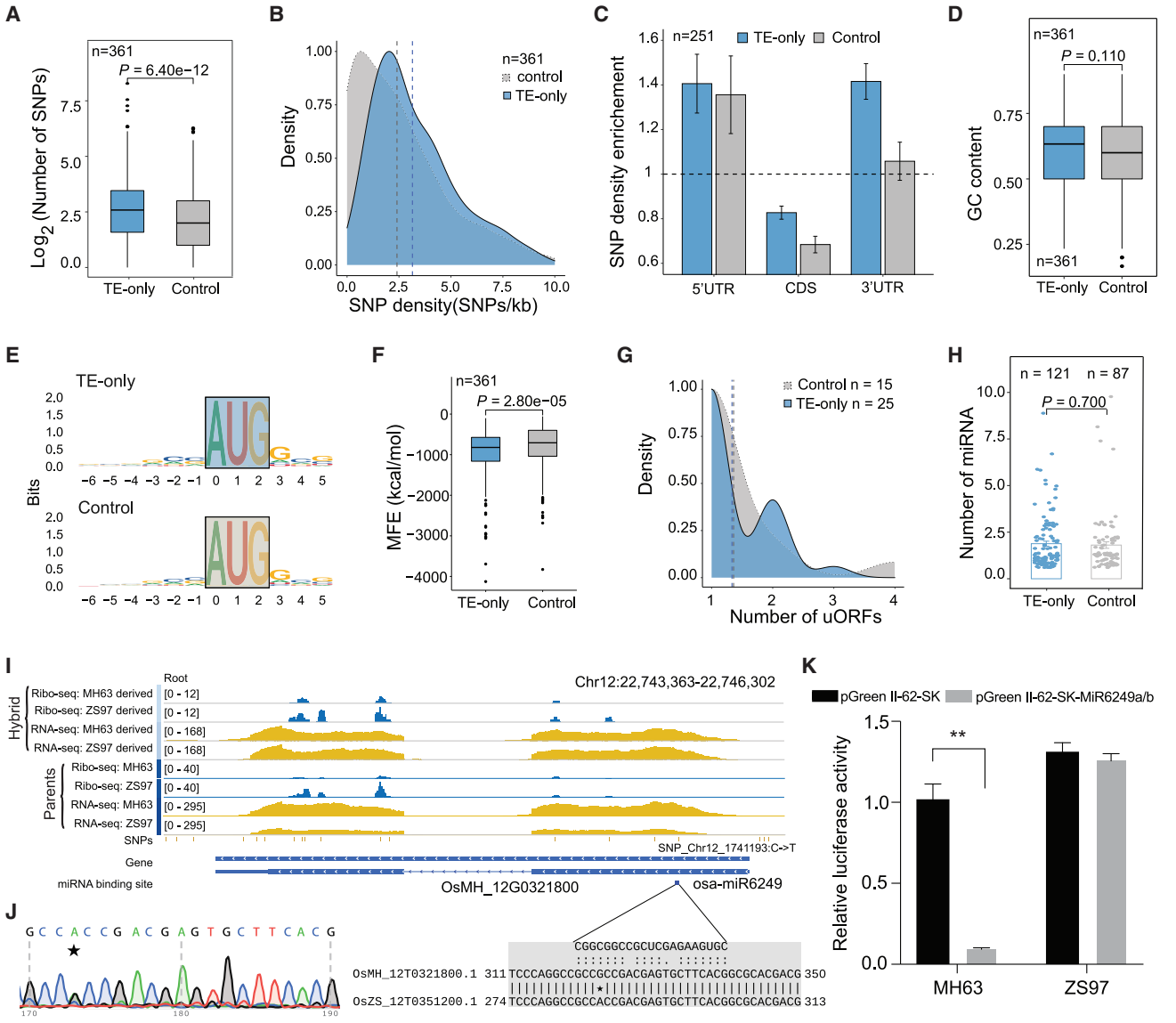

Figure 6. Effect of *cis*-regulatory elements on TE-only genes.

TE-only genes and control genes (those without TE divergence between alleles) are compared.

(A) Total number of SNPs.

(B) SNP density (SNPs/kb).

(C) Enrichment of SNPs among three features. Only genes with completely annotated structures (5′ UTR, CDS, and 3′ UTR) were used (n = 251). The SNP density enrichment (y axis) was calculated as the ratio of SNP density in each feature to the overall SNP density of each gene. Error bars display ±SEM.

(D) GC content around the start codon.

(E) Kozak sequence around the start codon.

(F) Minimum free energy (MFE), which reflects the secondary structure of mRNAs.

(G) uORF density. Only genes with uORFs were used for comparison (n = 25 and 15 for TE-only and control genes, respectively).

(H) Numbers of miRNA binding sites. Only genes with miRNA binding sites were used for comparison (n = 121 and 87 for TE-only and control genes, respectively).

(A, D, F, and H) Wilcoxon test *P* values are labeled.

(I) Difference in miRNA binding sites could potentially contribute to TE divergence in *OsMH_12G0321800*. Ribo-seq and RNA-seq from phased reads of hybrid and parents are shown in the first eight tracks, followed by SNPs, gene structure, and miRNA binding site tracks. The mature sequence of osa-miR6249 and target sites of MH63 and ZS97 alleles are shown at the bottom. An asterisk marks the SNP position in the target site between the two alleles.

(J) Sanger sequencing validated the true heterozygous status of the SNP in **(I)** in hybrid plant SY63. Two peaks with equal height represent adenine (green) and guanine (black).

(K) The relative luciferase activity for alleles *OsMH_12G0321800* and *OsZS_12G0351200* in protoplasts of hybrid SY63. Luciferase activity was significantly suppressed in the MH63 allele but not in the ZS97 allele, indicating that binding of miRNA osa-miR6249 only occurred in the former. Black and gray bars represent the control (null vector) and miRNA vector. Error bars display ±SEM. n = 3; $^{**}P \leq 0.01$ (Student's *t*-test).

transition from vegetative to reproductive growth in rice, and numerous key genes change their expression behavior at this time (Ke et al., 2018). These differences in the translatome are closely associated with the unique attributes of specific tissues. Not all uORFs repress translation of mORFs, as reported recently in the embryos of *D. melanogaster* (Patraquim et al., 2020) and maize (Chotewutmontri and Barkan, 2021), indicating a passive "bystander" role in which mORF translation is independent of uORFs as a result of the relatively high TE of the mORFs (Patraquim et al., 2020). In the present study, only a very small proportion of lncRNAs were translated and functionally annotated in rice, making it a greater challenge to dissect the roles of most of the rest.

Allelic TE divergence in the hybrid variety SY63 was another major focus of this study, and in general, TE-only genes showed higher mRNA abundance across tissues (Figure 5B and Supplemental Figure 10D and 10E). It is somewhat intuitive that, for translational regulation to trigger large effects, there must be a higher content of regulatory substrates, that is, higher total mRNA abundance. Some studies, for example in *Saccharomyces cerevisiae* (Li et al., 2017), have confirmed that translational regulation is dependent on mRNA amount to some extent. This phenomenon may be specific to allelic-specific translational regulation. A higher total mRNA level of genes with allelic TE divergence has also been observed in mice (Hou et al., 2015), indicating that allele-specific translational regulation is dependent on mRNA levels in animals and plants. Another interesting bias of TE-only genes was the apparent difference in the number of TE-only genes across tissues, with a markedly higher number in the root compared with the leaf and panicle. We speculated that this might reflect adaptation of the root to a more complex local developmental environment. Exposure of roots to the culture solution rather than the air, as for leaves and panicles, may necessitate some degree of translational regulation of specific genes. Apart from translation-related functions, some unique enriched GO terms of TE-only genes in the root, such as "response to osmotic stress" (GO: 0006970; $P = 2.87e{-}05$), also supported this hypothesis. Many investigated mRNA features showed no significant difference between TE-only genes and those without TE divergence (Supplemental Table 5). This might be explained by the relatively small effect of individual features on TE (Eichhorn et al., 2014) or by inaccurate prediction of *cis*-regulatory elements such as miRNA binding sites, which precluded comparisons from achieving statistical significance (Hou et al., 2015).

We suggest that future research may be focused on several of the following topics. First, about a decade ago, Brawand et al. (2011) investigated the evolution of gene expression in mammals using RNA-seq data and found that the evolutionary rate varied among different lineages and tissues. Recently, using the same materials plus Ribo-seq data, they demonstrated a co-evolutionary pattern of the transcriptome and translatome in mammals (Wang et al., 2020). One important reason for the success of their study was the innovation in algorithms for measuring the evolution of gene expression at the transcriptional and translational levels. To date, Ribo-seq and corresponding RNA-seq data have become available for several important monocots and dicots, such as *Arabidopsis* (Juntawong et al., 2014; Hsu et al., 2016; Bazin et al., 2017), maize (Lei et al., 2015), wheat (Guo et al., 2015), soybean (Shamimuzzaman and Vodkin, 2018), potato (Wu et al., 2019), and rice (Xiong et al., 2020), providing valuable resources for studying the evolution of genes at the transcriptional and translational levels in plants (Voelckel et al., 2017). However, in the long history after the divergence of animals and plants, plants have acquired many distinct genomic and morphological features totally different from those of animals. Hence, more new and robust algorithms are required to dissect the evolutionary history of plants at the translational level. Second, when evaluating the effect of *cis*-regulatory elements on allelic TE divergence, we mainly considered mRNA sequence features such as uORFs within the 5′ UTR and miRNA binding sites. However, we ignored another important factor, epigenetic mRNA modifications such as N6-methyladenosine (m6A) methylation, which are currently a fascinating research hotspot in plant mRNA studies. Many studies of mammals have revealed that m6A modification can mediate multiple biological processes, such as mRNA degradation, stability, and, most importantly, translation (Visvanathan and Somasundaram, 2018). However, such studies are still relatively rare in plants, and most of the available studies are focused mainly on the roles of m6A modification in plant development (Růžička et al., 2017) and stress response (Scutenaire et al., 2018). Whether these mRNA modifications also contribute to allelic TE divergence remains to be explored. Last but not least, as one of the most complex issues in plant biology research, heterosis has been attracting attention for more than 100 years because of its great significance in crop breeding (Schnable and Springer, 2013). With the availability of methods for quantifying gene expression levels, such as gene expression microarrays and RNA-seq, breeders can validate many modes of gene action, such as additivity and under- or over-dominance (Hochholdinger and Hoecker, 2007). However, very little research has been conducted on allele-specific expression at the translational level (Zhu et al., 2021). Neglect of heterosis at the translational level in previous studies is probably due to the intrinsic complexity of heterosis, as the observed heterosis cannot easily be explained by a single mechanism. Despite such great difficulties, we still observed two major regulatory patterns at the TE level, which accounted for more than 80% of TE-only genes, by comparing the variations at the transcriptional and translational levels between the parents and hybrid (Figure 5F). These two patterns only showed divergence at the TE level, highlighting the potentially important role of translational regulation in heterosis, which cannot easily be inferred using RNA-seq data only. Although pattern A can be primarily attributed to the inheritance by hybrid progeny of *cis*-regulatory variations from their parents, the mechanisms behind pattern B are somewhat more arcane. Differences in *trans*-acting factors that influence translation, like miRNAs, between parents and hybrid (Chen, 2013) as well as variations in some post-transcriptional epigenetic modifications at the mRNA level, like m6A (Xu et al., 2021), may lead to biased translation of one allele compared with its counterpart in the hybrid. More innovative experimental methods may be developed to help explore this phenomenon in more detail, thereby enhancing our understanding of the mechanism of heterosis and facilitating crop breeding for food safety.

By combining Ribo-seq and RNA-seq data from three tissues of three rice varieties, we obtained a comprehensive translational

profile that highlights the variations in translational regulation among tissues. By taking advantage of the hybrid and its parents, this study provides a first glimpse into allele-specific translational regulation in plants, which may have great significance for expanding our knowledge of crop breeding.

METHODS

Plant materials, library construction, and routine data processing

The seeds of three rice varieties, MH63, ZS97, and SY63, were first germinated by soaking in sterile water for 2 days and then transferred to a light incubator for growth under normal conditions (28°C for 14 h in the light and 26°C for 10 h in the dark, 70% humidity) in culture solution (Yoshida, 1976). Samples of young leaves and roots at the four-leaf stage and panicles were collected for RNA-seq and Ribo-seq library construction. All fresh samples were immediately frozen in −80°C liquid nitrogen until use. RNA-seq library construction and sequencing were performed as described in our earlier work (Zhou et al., 2021). The details of Ribo-seq library construction are described in Supplemental Methods 1. Multiple routine tools were used to process the RNA-seq and Ribo-seq data, and the details can be found in Supplemental Methods 2.

Analysis of unique features of Ribo-seq data

General features, such as length and genome distribution of RPFs, were calculated using custom R scripts. The P-site offset for each read length was determined with the psite command in Plastid (v.0.4.8) (Dunn and Weissman, 2016), and RPFs with a length of 25–31 nt were used for subsequent analysis. The 15th base from the 5′ end of reads was considered to be a simulated P-site offset while using RNA-seq as the control. Then riboWaltz (Lauria et al., 2018) was used to calculate the distribution of the P-site signal among the 5′ UTR, CDS, and 3′ UTR regions. For analysis of 3-nt periodicity, we first summed up the P site across every position of all mRNAs and then normalized the data with the average value of the upstream 20 bases from the start codon. The relative codon usage in Supplemental Figures 1D, 8B, and 12C was calculated in CodonW (v.1.4.2; http://codonw.sourceforge.net/) with the respective genes.

Calculation of TE and expression distance

The TE for each gene with a TPM value equal to or greater than 0.1 at both levels was defined as the ratio of $TPM_{Ribo\text{-}seq}$ to $TPM_{RNA\text{-}seq}$, and the TE range across genes in each sample was calculated as the ratio of the 97.5th to the 2.5th percentile of TEs to eliminate the effects of outliers. The expression variances were calculated from the expression matrix in R (Team, 2012), and the divergence in expression profile (expression distance) between a pair of tissues was measured by the Euclidean distance (Glazko and Mushegian, 2010): $d(m, n) = \sqrt{\sum_{i=1}^{N} [log_{10}(x_i+1) - log_{10}(y_i+1)]^2}/N$. In the equation, m and n refer to samples m and n; the variables x and y are the TPM values for gene i at the transcriptional or translational level in samples m and n, respectively; and the variable N represents the number of transcribed genes (N = 23 957) in all three varieties. A larger $d(m, n)$ indicates a greater variation in expression profile.

Identification of uORFs

uORFs longer than 10 aa were identified with an AUG start codon followed by an in-frame stop codon within the annotated 5′ UTR of primary protein-coding mRNAs in MH63RS3. ORFs completely contained within another were discarded. The sequenced reads mapped to uORFs were then counted with featureCounts (v.2.0.0) (Liao et al., 2014). ORFs with RPFs greater than three in any replicates were considered active uORFs in each sample. We downloaded all rice datasets of TFs from PlantTFDB (v.5.0) (Tian et al., 2020) to analyze the TF types of uORF-containing genes.

Detection and *de novo* functional annotation of actively translated ORFs in lncRNAs

The detection of actively translated ORFs was performed using RiboTaper (v.1.3.1a) (Calviello et al., 2016) with pairing RPF length and P-site offset: 25, 26, 27, 28, 29, 30, and 31 and 9, 10, 11, 12, 13, 13, and 13. ORFs with the same stop codon but different start codons were regarded as the same ORF across samples. The lncRNAs in the MH63RS3 genome were re-identified with the same pipeline described in our previous work (Zhou et al., 2021). Three strategies were used for *de novo* functional annotation of active ORFs. First, each putative active ORF was queried against multiple databases through a local InterProScan 5 (v.5.48-83.0) (Jones et al., 2014) with a hit e value threshold of 1e−5. Second, all annotated protein sequences in MH63RS3 with lengths shorter than 100 aa were treated as the set of known small proteins. The active ORFs were queried against this database using BLASTP (v.2.9.0+) (Camacho et al., 2009) with an e value threshold of 1e−5. Third, TMHMM 2 (Krogh et al., 2001) and SignalP-5.0 (Almagro Armenteros et al., 2019) were used with default parameters to predict transmembrane proteins and signal peptides. sORFs were first selected from protein-coding genes with CDSs shorter than 300 nt, and only those with translational activity predicted by RiboTaper were retained. The control sets were randomly selected from actively translated genes with CDSs longer than 300 nt, and the number was the same as that of the sORFs identified above.

Read phasing and identification of genes with ASTE

To identify genes with ASTE, it is necessary to distinguish reads derived from different parents. Previous studies in yeast (Artieri and Fraser, 2014) and mice (Hou et al., 2015) adopted the perfect matching strategy for read phasing. In this strategy, the reads should be perfectly matched to the SNP position of either homologous gene, but the perfectly matched reliable reads in one parent should have a mismatch in the SNP position of the other parent. We used PP2PG (v.1.0) (Feng et al., 2021), which implements such an algorithm, to phase the reads of SY63. Before the reads were phased (Figure 5A), nucmer, delta-filter, and show-snps in the MUMmer4 package (v.4.0.0beta2) (Marçais et al., 2018) were used to call SNPs between the MH63RS3 and ZS97RS3 genomes, and a total of 1 757 026 SNPs were identified. To evaluate the phasing quality, we also applied the same procedure to the Ribo-seq and RNA-seq reads from MH63 and ZS97. The error rate, which benchmarks the proportion of reads in MH63 datasets that were wrongly assigned to ZS97 or vice versa, was defined as ZS97-derived reads / (MH63-derived reads + ZS97-derived reads) in MH63 datasets or MH63-derived reads / (MH63-derived reads + ZS97-derived reads) in ZS97 datasets. Another quality index, separation rate, was used to describe how many reads in the total datasets could be phased and was calculated as (MH63-derived reads + ZS97-derived reads) / (MH63-derived reads + ZS97-derived reads + unknown reads). The phasing results are listed in Supplemental Table 4 and Supplemental Data 6.

After acquiring the phased reads, we used the intersect subcommand in Bedtools (v.2.28.0) (Quinlan and Hall, 2010) to select 14 659 genes from all 1:1 orthologs between the MH63 and ZS97 genomes that contained SNPs within their CDS regions and could thus be used to determine the allelic origin of reads that mapped to them. Next, featureCounts (v.2.0.0) (Liao et al., 2014) was used to assign the phased reads to these genes, and two read-count matrices could be constructed at the transcriptional and translational levels. Finally, we modified the R scripts in deltaTE (Chothani et al., 2019) and used DESeq2 (Love et al., 2014) to identify genes with significant differences in transcription as well as TE levels under a FDR $\leq$ 0.05 and $|\log_2(\text{fold change})| \geq 1$ cutoff. According to the $\log_2$(fold change) values at the transcriptional and TE levels, genes with allelic expression divergence were divided into four categories: genes whose expression changed only at the mRNA level (mRNA-only

genes) or only at the TE level (TE-only genes), compensatory genes, and reinforcing genes. The two alleles of mRNA-only genes differ only at the transcriptional level, but their TEs are not significantly different. Similarly, the two alleles of TE-only genes differ only in TE, but there is no significant difference at the transcriptional level. All of these analyses were performed with a custom R script.

Identification of *cis*-regulatory elements

Several mRNA sequence features were identified in this study. First, the SNPs called in the previous step were transferred from the genomic position to the mRNA position by the R package GenomicFeatures (v.1.40.1) (Lawrence et al., 2013). To reveal the unique features of TE-only genes, we randomly selected an equal number of homologous genes without TE divergence in a pair of alleles as the control genes. The SNP number, enriched density, distribution in different features, and density before the start codon were calculated using a custom R script. Second, the GC content of 30 bases around the start codon (–15, +14 bases) and the Kozak sequence (defined as the sequence from –6 to +5 bases relative to the start codon) for each involved gene was calculated or extracted using Bedtools. Third, RNAfold (v.2.4.16) (Lorenz et al., 2011) was used to calculate the MFE around the start codon (–15, +14 bases) with default parameters at a temperature of 28°C. The secondary structure in Supplemental Figure 12E was predicted using MXfold2 (Sato et al., 2021) with the default setting. Finally, to obtain highly reliable miRNA binding sites, we downloaded all mature rice miRNA sequences from miRBase (release 22) (Kozomara et al., 2019), and only the binding sites predicted by TargetFinder (https://github.com/carringtonlab/TargetFinder) and psRNAtarget (2017) (Dai et al., 2018) were retained for comparison analysis. The TE-only and control genes from the MH63 parent were used for the comparison in Figure 6D–6H.

GO enrichment analysis

We improved the functional annotation of genes in the MH63RS3 genome (Supplemental Methods 3), and the script run_GOseq.pl in the Trinity package (v.2.8.5) (Haas et al., 2013) was used for GO enrichment analysis.

Statistical methods

Fisher's exact test, Wilcoxon test, Kolmogorov–Smirnov test, and Pearson correlation coefficient calculation were performed using fisher.test, wilcox.test, ks.test, and cor.test in R, respectively. Additional data processing and plotting methods are described in Supplemental Methods 5.

SUPPLEMENTAL INFORMATION

Supplemental information is available at *Plant Communications Online*.

ACCESSION NUMBERS

The RNA-seq (GSA: CRA002886) and Ribo-seq (GSA: CRA008350) data reported in this paper have been deposited in the Genome Sequence Archive (GSA) (Chen et al., 2021) in the National Genomics Data Center (CNCB-NGDC Members and Partners, 2022), China National Center for Bioinformation/Beijing Institute of Genomics, Chinese Academy of Sciences, and are publicly accessible at https://ngdc.cncb.ac.cn/gsa. The Ribo-seq data can also be found at the GenBank database under the accession number PRJNA725700. The custom R scripts used in this study are freely available from GitHub at https://github.com/Zhuxitong/Rice_Ribo-seq.

FUNDING

This work was supported by the National Natural Science Foundation of China (31871269 and 32270712), the Hubei Provincial Natural Science Foundation of China (2019CFA014), and a starting research grant for High-level Talents from Guangxi University.

AUTHOR CONTRIBUTIONS

L.-L.C., J.-X.G., X.-T.Z., and R.Z. designed the project. X.-T.Z., R.Z., Y.-Y.Z., and J.-W.F. analyzed the data. X.-T.Z., R.Z., and J.C. performed the experiments. X.-T.Z., R.Z., M.T.u.Q., J.-W.Z., J.-X.G., and L.-L.C. wrote and revised the paper.

ACKNOWLEDGMENTS

We thank the National Key Laboratory of Crop Genetic Improvement, Huazhong Agricultural University for providing the bioinformatics computing resources. No conflict of interest is declared.

Received: April 21, 2022
Revised: August 23, 2022
Accepted: October 1, 2022
Published: October 4, 2022

REFERENCES

Almagro Armenteros, J.J., Tsirigos, K.D., Sønderby, C.K., Petersen, T.N., Winther, O., Brunak, S., von Heijne, G., and Nielsen, H. (2019). SignalP 5.0 improves signal peptide predictions using deep neural networks. Nat. Biotechnol. **37**:420–423.

Artieri, C.G., and Fraser, H.B. (2014). Evolution at two levels of gene expression in yeast. Genome Res. **24**:411–421.

Battle, A., Khan, Z., Wang, S.H., Mitrano, A., Ford, M.J., Pritchard, J.K., and Gilad, Y. (2015). Impact of regulatory variation from RNA to protein. Science **347**:664–667.

Bazin, J., Baerenfaller, K., Gosai, S.J., Gregory, B.D., Crespi, M., and Bailey-Serres, J. (2017). Global analysis of ribosome-associated noncoding RNAs unveils new modes of translational regulation. Proc. Natl. Acad. Sci. USA **114**:E10018–E10027.

Brar, G.A., and Weissman, J.S. (2015). Ribosome profiling reveals the what, when, where and how of protein synthesis. Nat. Rev. Mol. Cell Biol. **16**:651–664.

Brawand, D., Soumillon, M., Necsulea, A., Julien, P., Csárdi, G., Harrigan, P., Weier, M., Liechti, A., Aximu-Petri, A., Kircher, M., et al. (2011). The evolution of gene expression levels in mammalian organs. Nature **478**:343–348.

Brodersen, P., Sakvarelidze-Achard, L., Bruun-Rasmussen, M., Dunoyer, P., Yamamoto, Y.Y., Sieburth, L., and Voinnet, O. (2008). Widespread translational inhibition by plant miRNAs and siRNAs. Science **320**:1185–1190.

Calviello, L., Mukherjee, N., Wyler, E., Zauber, H., Hirsekorn, A., Selbach, M., Landthaler, M., Obermayer, B., and Ohler, U. (2016). Detecting actively translated open reading frames in ribosome profiling data. Nat. Methods **13**:165–170.

Calvo, S.E., Pagliarini, D.J., and Mootha, V.K. (2009). Upstream open reading frames cause widespread reduction of protein expression and are polymorphic among humans. Proc. Natl. Acad. Sci. USA **106**:7507–7512.

Camacho, C., Coulouris, G., Avagyan, V., Ma, N., Papadopoulos, J., Bealer, K., and Madden, T.L. (2009). BLAST+: architecture and applications. BMC Bioinf. **10**:421.

Cardoso-Moreira, M., Halbert, J., Valloton, D., Velten, B., Chen, C., Shao, Y., Liechti, A., Ascenção, K., Rummel, C., Ovchinnikova, S., et al. (2009). Gene expression across mammalian organ development. Nature **571**:505–509.

Chen, T., Chen, X., Zhang, S., Zhu, J., Tang, B., Wang, A., Dong, L., Zhang, Z., Yu, C., Sun, Y., et al. (2021). The genome sequence archive family: toward explosive data growth and diverse data types. Dev. Reprod. Biol. **19**:578–583.

Chen, Z.J. (2013). Genomic and epigenetic insights into the molecular bases of heterosis. Nat. Rev. Genet. **14**:471–482.

Chotewutmontri, P., and Barkan, A. (2021). Ribosome profiling elucidates differential gene expression in bundle sheath and mesophyll cells in maize. Plant Physiol. **187**:59–72.

Chothani, S., Adami, E., Ouyang, J.F., Viswanathan, S., Hubner, N., Cook, S.A., Schafer, S., and Rackham, O.J.L. (2019). deltaTE: detection of translationally regulated genes by integrative analysis of Ribo-seq and RNA-seq data. Curr. Protoc. Mol. Biol. **129**:e108.

Clark, J.W., and Donoghue, P.C.J. (2018). Whole-genome duplication and plant macroevolution. Trends Plant Sci. **23**:933–945.

Crick, F. (1970). Central dogma of molecular biology. Nature **227**:561–563.

Csárdi, G., Franks, A., Choi, D.S., Airoldi, E.M., and Drummond, D.A. (2015). Accounting for experimental noise reveals that mRNA levels, amplified by post-transcriptional processes, largely determine steady-state protein levels in yeast. PLoS Genet. **11**:e1005206.

Dai, X., Zhuang, Z., and Zhao, P.X. (2018). psRNATarget: a plant small RNA target analysis server (2017 release). Nucleic Acids Res. **46**:W49–W54.

Dunn, J.G., and Weissman, J.S. (2016). Plastid: nucleotide-resolution analysis of next-generation sequencing and genomics data. BMC Genom. **17**:958.

Dunn, J.G., Foo, C.K., Belletier, N.G., Gavis, E.R., and Weissman, J.S. (2013). Ribosome profiling reveals pervasive and regulated stop codon readthrough in *Drosophila melanogaster*. Elife **2**:e01179.

Eichhorn, S.W., Guo, H., McGeary, S.E., Rodriguez-Mias, R.A., Shin, C., Baek, D., Hsu, S.H., Ghoshal, K., Villén, J., and Bartel, D.P. (2014). mRNA destabilization is the dominant effect of mammalian microRNAs by the time substantial repression ensues. Mol. Cell **56**:104–115.

Feng, J.-W., Lu, Y., Shao, L., Zhang, J., Li, H., and Chen, L.-L. (2021). Phasing analysis of the transcriptome and epigenome in a rice hybrid reveals the inheritance and difference in DNA methylation and allelic transcription regulation. Plant Commun. **2**:100185.

Fields, A.P., Rodriguez, E.H., Jovanovic, M., Stern-Ginossar, N., Haas, B.J., Mertins, P., Raychowdhury, R., Hacohen, N., Carr, S.A., Ingolia, N.T., et al. (2015). A regression-based analysis of ribosome-profiling data reveals a conserved complexity to mammalian translation. Mol. Cell **60**:816–827.

Glazko, G., and Mushegian, A. (2010). Measuring gene expression divergence: the distance to keep. Biol. Direct **5**:51.

Guo, W., Zhang, J., Zhang, N., Xin, M., Peng, H., Hu, Z., Ni, Z., and Du, J. (2015). The wheat NAC transcription factor TaNAC2L is regulated at the transcriptional and post-translational levels and promotes heat stress tolerance in transgenic Arabidopsis. PLoS One **10**:e0135667.

Haas, B.J., Papanicolaou, A., Yassour, M., Grabherr, M., Blood, P.D., Bowden, J., Couger, M.B., Eccles, D., Li, B., Lieber, M., et al. (2013). De novo transcript sequence reconstruction from RNA-seq using the Trinity platform for reference generation and analysis. Nat. Protoc. **8**:1494–1512.

Hall, M.N., Gabay, J., Débarbouillé, M., and Schwartz, M. (1982). A role for mRNA secondary structure in the control of translation initiation. Nature **295**:616–618.

Hata, T., Satoh, S., Takada, N., Matsuo, M., and Obokata, J. (2021). Kozak sequence acts as a negative regulator for *de novo* transcription initiation of newborn coding sequences in the plant genome. Mol. Biol. Evol. **38**:2791–2803.

Hochholdinger, F., and Hoecker, N. (2007). Towards the molecular basis of heterosis. Trends Plant Sci. **12**:427–432.

Hou, J., Wang, X., McShane, E., Zauber, H., Sun, W., Selbach, M., and Chen, W. (2015). Extensive allele-specific translational regulation in hybrid mice. Mol. Syst. Biol. **11**:825.

Hsu, P.Y., Calviello, L., Wu, H.-Y.L., Li, F.-W., Rothfels, C.J., Ohler, U., and Benfey, P.N. (2016). Super-resolution ribosome profiling reveals unannotated translation events in *Arabidopsis*. Proc. Natl. Acad. Sci. USA **113**:E7126–E7135.

Ingolia, N.T. (2014). Ribosome profiling: new views of translation, from single codons to genome scale. Nat. Rev. Genet. **15**:205–213.

Ingolia, N.T., Brar, G.A., Rouskin, S., McGeachy, A.M., and Weissman, J.S. (2012). The ribosome profiling strategy for monitoring translation *in vivo* by deep sequencing of ribosome-protected mRNA fragments. Nat. Protoc. **7**:1534–1550.

Ingolia, N.T., Ghaemmaghami, S., Newman, J.R.S., and Weissman, J.S. (2009). Genome-wide analysis *in vivo* of translation with nucleotide resolution using ribosome profiling. Science **324**:218–223.

Iwakawa, H.-o., and Tomari, Y. (2013). Molecular insights into microRNA-mediated translational repression in plants. Mol. Cell **52**:591–601.

Jia, J., Lu, W., Liu, B., Yu, Y., Jin, X., Shu, Y., Long, Y., and Zhai, J. (2022). An atlas of plant full-length RNA reveals tissue-specific and evolutionarily-conserved regulation of poly(A) tail length. Preprint at bioRxiv. https://doi.org/10.1101/2022.01.21.477033.

Jones, P., Binns, D., Chang, H.-Y., Fraser, M., Li, W., McAnulla, C., McWilliam, H., Maslen, J., Mitchell, A., Nuka, G., et al. (2014). InterProScan 5: genome-scale protein function classification. Bioinformatics **30**:1236–1240.

Juntawong, P., Girke, T., Bazin, J., and Bailey-Serres, J. (2014). Translational dynamics revealed by genome-wide profiling of ribosome footprints in *Arabidopsis*. Proc. Natl. Acad. Sci. USA **111**:E203–E212.

Kang, K., Shim, Y., Gi, E., An, G., and Paek, N.-C. (2019). Mutation of ONAC096 enhances grain yield by increasing panicle number and delaying leaf senescence during grain filling in rice. Int. J. Mol. Sci. **20**:5241.

Kaur, R., Bhunia, R.K., and Rajam, M.V. (2020). MicroRNAs as potential targets for improving rice yield via plant architecture modulation: recent studies and future perspectives. J. Biosci. **45**:116.

Ke, S., Liu, X.J., Luan, X., Yang, W., Zhu, H., Liu, G., Zhang, G., and Wang, S. (2018). Genome-wide transcriptome profiling provides insights into panicle development of rice (*Oryza sativa* L.). Gene **675**:285–300.

Klepikova, A.V., and Penin, A.A. (2019). Gene expression maps in plants: current state and prospects. Plants **8**:309.

Kozak, M. (1987). An analysis of 5'-noncoding sequences from 699 vertebrate messenger RNAs. Nucleic Acids Res. **15**:8125–8148.

Kozomara, A., Birgaoanu, M., and Griffiths-Jones, S. (2019). miRBase: from microRNA sequences to function. Nucleic Acids Res. **47**:D155–D162.

Krogh, A., Larsson, B., Von Heijne, G., and Sonnhammer, E.L. (2001). Predicting transmembrane protein topology with a hidden Markov model: application to complete genomes. J. Mol. Biol. **305**:567–580.

Lauria, F., Tebaldi, T., Bernabò, P., Groen, E.J.N., Gillingwater, T.H., and Viero, G. (2018). riboWaltz: optimization of ribosome P-site positioning in ribosome profiling data. PLoS Comput. Biol. **14**:e1006169.

Lawrence, M., Huber, W., Pagès, H., Aboyoun, P., Carlson, M., Gentleman, R., Morgan, M.T., and Carey, V.J. (2013). Software for computing and annotating genomic ranges. PLoS Comput. Biol. **9**:e1003118.

Lei, L., Shi, J., Chen, J., Zhang, M., Sun, S., Xie, S., Li, X., Zeng, B., Peng, L., Hauck, A., et al. (2015). Ribosome profiling reveals dynamic translational landscape in maize seedlings under drought stress. Plant J. **84**:1206–1218.

Li, G., Zhang, H., Li, J., Zhang, Z., and Li, Z. (2021). Genetic control of panicle architecture in rice. Crop J. **9**:590–597.

Li, J.J., Chew, G.L., and Biggin, M.D. (2017). Quantitating translational control: mRNA abundance-dependent and independent contributions and the mRNA sequences that specify them. Nucleic Acids Res. **45**:11821–11836.

Liao, Y., Smyth, G.K., and Shi, W. (2014). featureCounts: an efficient general purpose program for assigning sequence reads to genomic features. Bioinformatics **30**:923–930.

Liu, M.-J., Wu, S.-H., Wu, J.-F., Lin, W.-D., Wu, Y.-C., Tsai, T.-Y., Tsai, H.-L., and Wu, S.-H. (2013). Translational landscape of photomorphogenic *Arabidopsis*. Plant Cell **25**:3699–3710.

Lorenz, R., Bernhart, S.H., Höner Zu Siederdissen, C., Tafer, H., Flamm, C., Stadler, P.F., and Hofacker, I.L. (2011). ViennaRNA package 2.0. Algorithms Mol. Biol. **6**:26.

Love, M.I., Huber, W., and Anders, S. (2014). Moderated estimation of fold change and dispersion for RNA-seq data with DESeq2. Genome Biol. **215**:550.

Marçais, G., Delcher, A.L., Phillippy, A.M., Coston, R., Salzberg, S.L., and Zimin, A. (2018). MUMmer4: a fast and versatile genome alignment system. PLoS Comput. Biol. **14**:e1005944.

Marla, S.S., and Singh, V.K. (2012). LOX genes in blast fungus (*Magnaporthe grisea*) resistance in rice. Funct. Integr. Genomics **12**:265–275.

Matsubayashi, Y. (2014). Posttranslationally modified small-peptide signals in plants. Annu. Rev. Plant Biol. **65**:385–413.

McManus, C.J., May, G.E., Spealman, P., and Shteyman, A. (2014). Ribosome profiling reveals post-transcriptional buffering of divergent gene expression in yeast. Genome Res. **24**:422–430.

CNCB-NGDC Members and Partners. (2022). Database resources of the national genomics data center, China national center for bioinformation in 2022. Nucleic Acids Res. **50**:D27–D38.

Muzzey, D., Sherlock, G., and Weissman, J.S. (2014). Extensive and coordinated control of allele-specific expression by both transcription and translation in *Candida albicans*. Genome Res. **24**:963–973.

Noor, Z., Ahn, S.B., Baker, M.S., Ranganathan, S., and Mohamedali, A. (2021). Mass spectrometry–based protein identification in proteomics—a review. Brief. Bioinform. **22**:1620–1638.

Patraquim, P., Mumtaz, M.A.S., Pueyo, J.I., Aspden, J.L., and Couso, J.-P. (2020). Developmental regulation of canonical and small ORF translation from mRNAs. Genome Biol. **21**:128.

Puranik, S., Sahu, P.P., Srivastava, P.S., and Prasad, M. (2012). NAC proteins: regulation and role in stress tolerance. Trends Plant Sci. **17**:369–381.

Qi, Z., and Xiong, L. (2013). Characterization of a purine permease family gene Os PUP 7 involved in growth and development control in rice. J. Integr. Plant Biol. **55**:1119–1135.

Quinlan, A.R., and Hall, I.M. (2010). BEDTools: a flexible suite of utilities for comparing genomic features. Bioinformatics **26**:841–842.

Ribone, P.A., Capella, M., Arce, A.L., and Chan, R.L. (2017). A uORF represses the transcription factor AtHB1 in aerial tissues to avoid a deleterious phenotype. Plant Physiol. **175**:1238–1253.

Růžička, K., Zhang, M., Campilho, A., Bodi, Z., Kashif, M., Saleh, M., Eeckhout, D., El-Showk, S., Li, H., Zhong, S., et al. (2017). Identification of factors required for m6A mRNA methylation in Arabidopsis reveals a role for the conserved E3 ubiquitin ligase HAKAI. New Phytol. **215**:157–172.

Sato, K., Akiyama, M., and Sakakibara, Y. (2021). RNA secondary structure prediction using deep learning with thermodynamic integration. Nat. Commun. **12**:941.

Schnable, P.S., and Springer, N.M. (2013). Progress toward understanding heterosis in crop plants. Annu. Rev. Plant Biol. **64**:71–88.

Scutenaire, J., Deragon, J.-M., Jean, V., Benhamed, M., Raynaud, C., Favory, J.-J., Merret, R., and Bousquet-Antonelli, C. (2018). The YTH domain protein ECT2 is an m6A reader required for normal trichome branching in Arabidopsis. Plant Cell **30**:986–1005.

Shamimuzzaman, M., and Vodkin, L. (2018). Ribosome profiling reveals changes in translational status of soybean transcripts during immature cotyledon development. PLoS One **13**:e0194596.

Song, J.-M., Xie, W.-Z., Wang, S., Guo, Y.-X., Koo, D.-H., Kudrna, D., Gong, C., Huang, Y., Feng, J.-W., Zhang, W., et al. (2021). Two gap-free reference genomes and a global view of the centromere architecture in rice. Mol. Plant **14**:1757–1767.

Song, X., Li, Y., Cao, X., and Qi, Y. (2019). MicroRNAs and their regulatory roles in plant–environment interactions. Annu. Rev. Plant Biol. **70**:489–525.

Subtelny, A.O., Eichhorn, S.W., Chen, G.R., Sive, H., and Bartel, D.P. (2014). Poly(A)-tail profiling reveals an embryonic switch in translational control. Nature **508**:66–71.

Team, C.R. (2012). Team RDC. R: A Language and Environment for Statistical Computing (Vienna, Austria: R Foundation for Statistical Computing).

Tian, F., Yang, D.-C., Meng, Y.-Q., Jin, J., and Gao, G. (2020). PlantRegMap: charting functional regulatory maps in plants. Nucleic Acids Res. **48**:D1104–D1113.

Urquidi Camacho, R.A., Lokdarshi, A., and von Arnim, A.G. (2020). Translational gene regulation in plants: a green new deal. Wiley Interdiscip. Rev. RNA **11**:e1597.

Visvanathan, A., and Somasundaram, K. (2018). mRNA traffic control reviewed: N6-methyladenosine (m6A) takes the driver's seat. Bioessays **40**:1700093.

Voelckel, C., Gruenheit, N., and Lockhart, P. (2017). Evolutionary transcriptomics and proteomics: insight into plant adaptation. Trends Plant Sci. **22**:462–471.

Waldman, Y.Y., Tuller, T., Shlomi, T., Sharan, R., and Ruppin, E. (2010). Translation efficiency in humans: tissue specificity, global optimization and differences between developmental stages. Nucleic Acids Res. **38**:2964–2974.

Wang, L., and Roossinck, M.J. (2006). Comparative analysis of expressed sequences reveals a conserved pattern of optimal codon usage in plants. Plant Mol. Biol. **61**:699–710.

Wang, Z.-Y., Leushkin, E., Liechti, A., Ovchinnikova, S., Mößinger, K., Brüning, T., Rummel, C., Grützner, F., Cardoso-Moreira, M., Janich, P., et al. (2020). Transcriptome and translatome co-evolution in mammals. Nature **588**:642–647.

Weinberg, D.E., Shah, P., Eichhorn, S.W., Hussmann, J.A., Plotkin, J.B., and Bartel, D.P. (2016). Improved ribosome-footprint and mRNA measurements provide insights into dynamics and regulation of yeast translation. Cell Rep. **14**:1787–1799.

Wu, H.-Y.L., Song, G., Walley, J.W., and Hsu, P.Y. (2019). The tomato translational landscape revealed by transcriptome assembly and ribosome profiling. Plant Physiol. **181**:367–380.

Xie, F., and Zhang, J. (2018). Shanyou 63: an elite mega rice hybrid in China. Rice **11**:17.

Xiong, Q., Zhong, L., Du, J., Zhu, C., Peng, X., He, X., Fu, J., Ouyang, L., Bian, J., Hu, L., et al. (2020). Ribosome profiling reveals the effects of nitrogen application translational regulation of yield recovery after abrupt drought-flood alternation in rice. Plant Physiol. Biochem. **155**:42–58.

Xu, C.G., Li, X.Q., Xue, Y., Huang, Y.W., Gao, J., and Xing, Y.Z. (2004). Comparison of quantitative trait loci controlling seedling characteristics at two seedling stages using rice recombinant inbred lines. Theor. Appl. Genet. **109**:640–647.

Xu, Z., Shi, X., Bao, M., Song, X., Zhang, Y., Wang, H., Xie, H., Mao, F., Wang, S., Jin, H., et al. (2021). Transcriptome-wide analysis of RNA m6A methylation and gene expression changes among two Arabidopsis ecotypes and their reciprocal hybrids. Front. Plant Sci. **12**:685189.

Yang, X., Cui, J., Song, B., Yu, Y., Mo, B., and Liu, L. (2020). Construction of high-quality rice ribosome footprint library. Front. Plant Sci. **11**:572237.

Yoshida, S., Fomo, D.A., Cock, J.H., and Gomez, K.A. (1976). Routine procedure for growing rice plants in culture solution. In Laboratory Manual for Physiological Studies of Rice, S. Yoshida, D.A. Forno, and J.H. Cock, eds. (Los Baños: International Rice Research Institute), pp. 61–66.

Zhao, D., Hamilton, J.P., Hardigan, M., Yin, D., He, T., Vaillancourt, B., Reynoso, M., Pauluzzi, G., Funkhouser, S., Cui, Y., et al. (2017). Analysis of ribosome-associated mRNAs in rice reveals the importance of transcript size and GC content in translation. G3 (Bethesda) **7**:203–219.

Zhou, L., Cheung, M.-Y., Li, M.-W., Fu, Y., Sun, Z., Sun, S.-M., and Lam, H.-M. (2010). Rice hypersensitive induced reaction protein 1 (OsHIR1) associates with plasma membrane and triggers hypersensitive cell death. BMC Plant Biol. **10**:290–310.

Zhou, R., Sanz-Jimenez, P., Zhu, X.-T., Feng, J.-W., Shao, L., Song, J.-M., and Chen, L.-L. (2021). Analysis of rice transcriptome reveals the lncRNA/circRNA regulation in tissue development. Rice **14**:14.

Zhu, W., Chen, S., Zhang, T., Qian, J., Luo, Z., Zhao, H., Zhang, Y., and Li, L. (2021). Dynamic patterns of the translatome in a hybrid triplet show translational fractionation of the maize subgenomes. Crop J. **10**:36–46. https://doi.org/10.1016/j.cj.2021.02.002.